sustainability

MDPI

Article

Eco-Friendly Biosynthesis and Characterization of Silver Nanoparticles Using *Zinnia elegans* L. Plant Extracts

Ilona Jonuškienė [1,2,*], Justė Narmontaitė [1,3], Kristina Kantminienė [3], Ingrida Tumosienė [1], Rima Stankevičienė [1] and Neringa Petrašauskienė [3]

[1] Department of Organic Chemistry, Kaunas University of Technology, Radvilėnų Pl. 19, 50254 Kaunas, Lithuania; justenarmontaite@gmail.com (J.N.); ingrida.tumosiene@ktu.lt (I.T.); rima.stankeviciene@ktu.lt (R.S.)
[2] Bioprocess Research Centre, Kaunas University of Technology, Radvilėnų Pl. 19, 50254 Kaunas, Lithuania
[3] Department of Physical and Inorganic Chemistry, Kaunas University of Technology, Radvilėnų Pl. 19, 50254 Kaunas, Lithuania; kristina.kantminiene@ktu.lt (K.K.); neringa.petrasauskiene@ktu.lt (N.P.)
* Correspondence: ilona.jonuskiene@ktu.lt

Abstract

This research investigated the sustainable biosynthesis of silver nanoparticles (AgNPs) using *Zinnia elegans* L. extracts to demonstrate the potential of plant-based methods in nanotechnology. The antioxidant and antibacterial properties of the plant extracts were evaluated, and the phytocompounds that react as natural reducing agents in the synthesis of AgNPs were characterized. This approach has demonstrated the potential of *Zinnia elegans* L. as an environmentally friendly source for the production of AgNPs. The biosynthesized AgNPs were characterized based on their optical, structural, and morphological properties using various techniques, including scanning electron microscopy (SEM), attenuated total reflectance–Fourier transform infrared spectroscopy (ATR-FTIR), and thermogravimetric and differential thermal analysis (TGA/DTA). X-ray diffraction (XRD) analysis confirmed the presence of pure silver phases exhibiting a face-centered cubic (FCC) crystalline structure. Ultraviolet–visible (UV–Vis) spectroscopy revealed an absorption peak at 462 nm, which is characteristic of the surface plasmon resonance associated with AgNPs. ATR-FTIR analysis identified several vibrational peaks corresponding to the functional groups of the constituents present in the biosynthesized AgNPs. The size distribution of the AgNPs was found to range from 10 to 30 nm, and both SEM and TEM confirmed their predominantly spherical morphology. Energy dispersive X-ray spectroscopy (EDX) analysis corroborated the predominance of silver as the principal element within the composition of the nanoparticles. This technique provided quantitative elemental analysis, confirming the high purity and concentration of silver in the synthesized AgNPs. The study effectively elucidated the synthesis of AgNPs utilizing plant extracts as natural reducing agents. The synthesized AgNPs exhibited significant antibacterial and antioxidant activities, indicating their potential applicability in diverse biomedical and environmental contexts. Employment of the advanced characterization techniques facilitated a thorough understanding of the multifaceted properties of the synthesized AgNPs, thereby enhancing their viability for future research and application in nanomedicine and bioremediation. Using *Zinnia elegans* L. for the biosynthesis of plant-synthesized AgNPs is a sustainable and eco-friendly technique that offers a viable alternative to conventional chemical processes.

Academic Editor: Konstantinos Dimos

Received: 19 September 2025
Revised: 10 October 2025
Accepted: 21 October 2025
Published: date

Citation: Jonuškienė, I.; Narmontaitė, J.; Kantminienė, K.; Tumosienė, I.; Stankevičienė, R.; Petrašauskienė, N. Eco-Friendly Biosynthesis and Characterization of Silver Nanoparticles Using *Zinnia elegans* L. Plant Extracts. *Sustainability* **2025**, *17*, x. https://doi.org/10.3390/xxxxx

Keywords: biosynthesis; phytochemicals; silver nanoparticles; antioxidant activity; bioprocessing

1. Introduction

The expanding demand for eco-friendly and biocompatible nanomaterials has led to a focus on green synthesis methods that utilize plant-based resources. *Zinnia elegans* L. is a highly valued and versatile ornamental plant with significant potential for various horticultural and environmental applications. Its diverse flower forms, ease of cultivation, and ability to adapt to different conditions make it a staple of ornamental horticulture. Several varieties and cultivars have been developed and studied for their unique traits and adaptability. *Zinnia elegans* L., a member of the *Asteraceae* family, includes 20 annual and perennial plant species found in South America and Mexico [1]. *Zinnia elegans* L., an annual, fast-growing, flowering plant with high biomass, is primarily cultivated for its flowers and production of natural dyes. *Zinnia elegans* L. holds significant potential as a source of bioactive secondary metabolites with various therapeutic properties [2,3].

Studies have shown that *Zinnia elegans* L. exhibits a variety of biological properties, including antioxidant [3], antifungal [4], antibacterial [5], antimalarial [4], and cytotoxic [6] properties. *Zinnia elegans* L. contains various bioactive secondary metabolites, such as phenolic acids and flavonoids [7]. These compounds promote the plant's biological activities, enhancing its potential as a reducing and stabilizing substance in nanoparticle synthesis. Phenolic compounds, including phenolic acids and flavonoids, are known for their strong antioxidant and redox properties [3]. This enables them to donate electrons and reduce metal ions during the formation of nanoparticles. Flavonoids, including quercetin and luteolin derivatives, participate in the reduction process and act as natural capping substances. These agents stabilize the surface of synthesized nanoparticles, influencing their size and morphology. These phytochemicals have also been associated with various biological effects, including anti-inflammatory, antimicrobial, and anticancer properties [8]. These findings further reinforce the idea that AgNPs synthesized from *Zinnia elegans* L. could be used to promote environmentally sustainable strategies in environmental biotechnology and antibacterial treatment [6]. The methanolic extract of *Zinnia elegans* L. is rich in phenolic compounds and exhibits greater antioxidant activity than other extracts obtained using chloroform or *n*-hexane. This suggests that the antioxidant activity is due to its high polyphenol content [4]. Studies have also confirmed the presence of saponins, tannins, and quinones as phytochemicals along with other terpenoids in *Zinnia elegans* L. leaves [9]. While initial studies have identified several promising compounds, further research and innovative strategies are essential to overcome existing challenges and fully realize their medical applications. Plant cell cultures have also demonstrated the potential to synthesize phytopharmaceuticals with biological activity. In this regard, *Zinnia elegans* L. has been investigated as a source of bioactive phytometabolites using in vitro callus cultures.

Nanotechnology involving metal nanoparticles has found broad applications in various scientific and technological fields, including the biomedical sciences. This advanced technology is attributed to the distinctive physical–chemical traits of nanoparticles, which are defined by their size and shape. Based on their special antimicrobial, optical, and catalytic features, AgNPs have been widely used in various fields, including medicine, agriculture, environmental science, and industry. In the biomedicinal field, AgNPs are predominantly used for their antimicrobial properties since they are effective against a broad spectrum of microorganisms and viruses. They are used in protective coatings for medical devices, diagnostic tools, and drug nanodelivery systems [10–14]. In agriculture, AgNPs

improve the efficacy of pesticides and fertilizers, while protecting crops against pathogens [15,16]. In environmental applications, AgNPs play a crucial role in water purification and pollutant detection [14,17,18]. In the bioindustry, AgNPs function as catalysts in a variety of chemical reactions, including the degradation of synthetic dyes and the removal of polluting substances. This capability is attributable to their elevated surface area and reactivity [14,17,19]. AgNPs are also used in the production of electronic components and optical instruments due to their distinctive electrical and optical properties [19].

Conventional methods of synthesizing AgNPs involve hazardous chemicals, whereas advanced, eco-friendly synthesis has attracted considerable interest owing to cost-effective and non-toxic characteristics. This bioprocessing method uses plant extracts, microorganisms, and other bioresources as reducing agents, providing a biological alternative to traditional methods [20–23]. AgNPs obtained by green synthesis are widely used in health-related fields due to their antimicrobial and anticancer properties [20–22,24–28], as well as for wound healing [22]. They are also used in environmental applications, such as the monitoring and treatment of water pollution [29,30].

Despite extensive research on green synthesis using various plant extracts, little data exist on *Zinnia elegans* L. specifically. Only a few studies have investigated the use of *Zinnia elegans* L. leaf extract for AgNP biosynthesis, focusing exclusively on in vivo synthesis and evaluation [8]. The present study explores *Zinnia elegans* L. as a biosynthetic platform in both in vitro and in vivo (leaves, stems, and blossoms) contexts. These findings suggest the possibility of using AgNPs derived from bioresources as antibacterial agents and for studying antibiofilm activity in the future. Using *Zinnia elegans* L. for the biological synthesis of AgNPs is a sustainable and effective method with significant potential for biomedical applications, especially in cancer therapy and bioimaging.

The research evaluated the antioxidant and antibacterial properties of *Zinnia elegans* L. blossoms, leaves, and stems. It also examined the concentrations of biologically active compounds, such as phenolic compounds, phenolic acids, and flavonoids, in these extracts, as well as in leaf, stem, and root callus cultures. Additionally, AgNP biosynthesis was performed using *Zinnia elegans* L. plant extracts. The resulting AgNPs were characterized based on their optical, structural, and morphological properties. The characterization of the AgNPs included scanning electron microscopy (SEM), attenuated total reflectance–Fourier transform infrared spectroscopy (ATR-FTIR), and thermogravimetric and differential thermal analysis (TGA/DTA). The antibacterial activity of AgNPs against both Gram-positive and Gram-negative bacteria was also tested.

This study demonstrates the biological activity of *Zinnia elegans* L. plant extracts, as well as the sustainable production and characterization of plant-synthesized AgNPs. This environmentally friendly approach offers a bio-sustainable alternative to the usual methods and positions *Zinnia elegans* L. as a valuable resource in the growing field of advanced nanotechnology. Future research endeavors should focus on optimizing synthesis parameters and exploring the diverse functional properties of the synthesized AgNPs for applications in biomedicine, enzymology, environmental remediation, and beyond.

2. Materials and Methods

2.1. Materials and Methods

Pure analytical reagents and distilled water were used to prepare the solutions. All reagents were obtained from Sigma-Aldrich (St. Louis, MO, USA) and were used without modification.

Formation of callus cultures of *Zinnia elegans* L: The seeds were first washed with 70% ethanol solution for 60 s, followed by surface sterilization with 0.1% $HgCl_2$ for 10 min. Then, the seeds were rinsed three times with sterile deionized water. The seeds were

cultured on a Murashige and Skoog (MS) medium, supplemented with 6-benzylaminopurine (BAP) (1 mg/L) and 1-naphthylacetic acid (NAA) (1 mg/L) [31]. The callus culture cycle was maintained for 30 days under controlled conditions.

Preparation of *Zinnia elegans* L. plant extracts: The aerial parts of *Zinnia elegans* L. were collected in Kaunas, Lithuania. The blossoms, leaves, and stems were carefully separated, thoroughly washed with distilled water, and dried at 45 °C.

The ferric ion (Fe^{3+}) reducing antioxidant power was used. An increase in the absorbance of the reaction mixture corresponds to higher reducing power. This method was performed according to the literature [32].

The ferric ion reducing antioxidant power (FRAP) assay was performed. Antioxidant activity was determined according to the literature [32].

For the DPPH radical scavenging assay, the radical scavenging activity of Zinnia elegans L. plant extracts was measured using a method that was previously described in the literature [32]. Determination of the total phenolic content: The total phenolic content was determined by the Folin–Ciocalteu method [33].

Determination of the total phenolic acid content: Extraction was carried out according to the method described by Kvasnička et al. [34].

For the determination of the total flavonoid content, the aluminum chloride assay [35] was used.

Antibacterial activity studies: The agar diffusion method [26] was used to evaluate the antibacterial activity. Two bacterial species, *Escherichia coli* and *Bacillus subtilis*, were used as test organisms [23,27]. Ciprofloxacin was used as a positive control at a concentration of 12.5 μg/mL in all experiments.

Synthesis of AgNPs: AgNPs were synthesized using extracts of *Zinnia elegans* L. plant. The plant material (2.5 g) was homogenized in ultra-pure water (45 mL) and heated up to 60 °C for 40 min. The mixture was then filtered through Whatman No. 1 filter paper. The plant extract (5 mL) collected as filtrate was added to the aqueous $AgNO_3$ solution (2.5 mL, 1 M) to reduce Ag^+ ions. The $AgNO_3$ solution was freshly prepared and used on the same day. The reaction mixture was stirred at 100 rpm at 25 °C for 5 min. The pH of the solution was adjusted to 9 with 0.01 M NaOH. The AgNP synthesis reaction mixture was kept at room temperature for 24 h until the resulting solution turned dark brown. The solution was then centrifuged at 9000 rpm for 10 min using a Hettich Universal 320 centrifuge (Hettich GmbH & Co., Tuttlingen, Germany) and dried in air.

2.2. Characterization of AgNPs

XRD diffraction analysis of AgNPs: The biosynthesized AgNPs were characterized to study their phase and crystallinity using an X-ray diffractometer (D8 Advance diffractometer, Bruker AXS, Karlsruhe, Germany). The average crystallite size of the AgNPs was calculated using the Debye–Scherrer equation [36]. The experimental value(s) of d (lattice spacing) for the crystallite were determined using the Bragg relation [37]. The lattice parameters of the AgNP crystallites were calculated according to the equation previously described in the literature [38,39].

Optical properties of AgNPs: The optical absorption of the AgNPs was measured at room temperature using a Lambda 35 UV–Vis spectrometer (PerkinElmer Inc., Waltham, MA, USA) in the 380–700 nm range.

ATR-FTIR analysis of AgNPs: The presence of functional groups was confirmed using a Bruker ALPHA spectrometer (Bruker Optik GmbH, Ettlingen, Germany), which was equipped with attenuated total reflectance–Fourier transform infrared spectroscopy and a platinum ATR single reflection diamond module.

SEM/EDX and TEM/EDX analysis of AgNPs: The size and shape of the nanoparticles were studied using a scanning electron microscope (SEM, Carl Zeiss AG, Oberkochen,

Germany). Stoichiometric analysis was performed by energy-dispersive X-ray spectroscopy (EDX, Bruker Quantax 200, Bruker Nano GmbH, Berlin, Germany) coupled to SEM, and by transmission electron microscope (TEM, Tecnai G2 F20 X-TWIN, FEI Company, Eindhoven, The Netherlands) equipped with an EDX energy-dispersive X-ray spectrometer and r-TEM detector.

Thermogravimetric analysis: Thermogravimetric analysis (TGA) and differential thermal analysis (DTA) were performed to evaluate the thermal stability and composition of the biosynthesized AgNPs. The thermal stability and the loss of surface weight of the AgNPs were determined on a Linseis STA PT1600 thermal analyzer (Linseis Massgeraete GmbH, Selb, Germany). The TGA/DTA spectra were obtained under an N_2 atmosphere at a heating rate of 10 °C·min^{-1} within the temperature range of 30 to 930 °C.

Statistical analysis: Statistically significant comparisons between *Zinnia elegans* L. plant in vivo extracts (from leaves and stems) and callus cultures (in vitro from leaves and stems) were carried out with an unpaired two-tailed *t*-test, with a significance level set at $p < 0.01$. GraphPad Prism version 8.0.2 for Windows (San Diego, CA, USA) was used [31].

3. Results and Discussion

This study examined the biochemical properties of *Zinnia elegans* L., including its antioxidant activity and phytocompound concentrations in its extracts. The antibacterial activity of plant extracts against selected bacteria was also investigated. Additionally, the biosynthesis of AgNPs using *Zinnia elegans* L. extracts was performed and fine-tuned. The resulting AgNPs were characterized based on their optical, structural, and morphological properties. Their antibacterial activity was also tested against chosen bacteria.

3.1. Biochemical Properties of Zinnia elegans L.

3.1.1. Antioxidant Activity

Antioxidants are defined as substances, either naturally occurring or synthetic, that are capable of preventing or retarding cell damage caused by reactive oxidants. These substances act at low concentrations and must effectively neutralize target radicals while producing less-toxic reaction products. It is important to note that a universal antioxidant does not exist. Rather, various antioxidants act on different reactive species through diverse mechanisms and in different cellular locations [40].

The reducing (antioxidant) properties of plant extracts are evaluated by assessing their ability to donate electrons and neutralize free radicals. These antioxidants can prevent oxidative damage to cells by removing harmful radicals. Several techniques have been used to evaluate antioxidant activity, including the ferric ion (Fe^{3+}) reducing antioxidant power determination assay, the DPPH radical scavenging assay, and the FRAP assay.

The method for the determination of the reducing (Fe^{3+}) antioxidant power of *Zinnia elegans* L. plant extracts measures how well antioxidants donate electrons. In the assay, the reduction of ferric ions (Fe^{3+}) to ferrous ions (Fe^{2+}) indicates reducing power. The color change indicates the formation of a Fe^{2+} complex, and absorbance is measured at 700 nm [32].

Evaluation of the reducing properties of *Zinnia elegans* L. blossom, leaf, and stem extracts demonstrated that the blossom extract exhibited the most significant reducing (i.e., antioxidant) properties (Figure 1). The absorbance of the blossom extract was 0.8 o.u. at 700 nm. In contrast, the stem extract exhibited the lowest absorbance of 0.2 o.u., suggesting that its reducing properties were the weakest among the extracts examined.

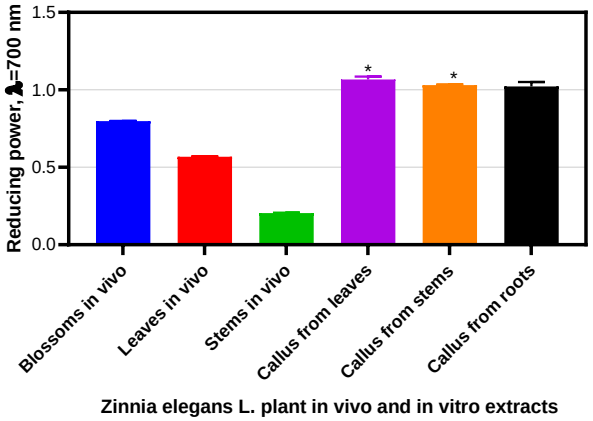

Figure 1. Reducing (antioxidant) properties of *Zinnia elegans* L. plant extracts. The error bars show the mean ± SD from three replicates. Asterisks show statistically significant comparisons between *Zinnia elegans* L. plant in vivo extracts (from leaves and stems) and callus cultures (from leaves and stems) in vitro were tested with an unpaired two-tailed *t*-test, with a significance level set at * $p <$ 0.01.

The reducing (antioxidant) power of the callus culture extracts from *Zinnia elegans* L. leaves, stems, and roots was 1.07, 1.03, and 1.02 o.u., respectively. The callus culture extracts from the leaves exhibited the highest reducing power activity (1.07 o.u.).

The antioxidant activity of *Zinnia elegans* L. plant extracts was evaluated by DPPH radical scavenging assay. This assay is a widely used method for evaluating the free radical scavenging capacity of different plant samples [41].

The results obtained (Figure 2) indicated that the callus culture extracts from the leaves, stems, and roots of *Zinnia elegans* L. exhibited DPPH inhibition values of 88.23%, 93.22%, and 91.92%, respectively. The most significant DPPH inhibition was observed for stem callus culture extracts, reaching 93.22%.

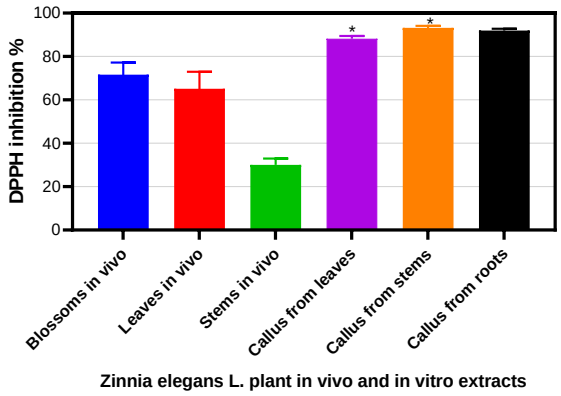

Figure 2. Antioxidative activity according to the DPPH assay of *Zinnia elegans* L. plant extracts. The error bars show the mean ± SD from three replicates. Asterisks show statistically significant comparisons between *Zinnia elegans* L. plant in vivo extracts (from leaves and stems) and callus cultures (from leaves and stems) in vitro were tested with an unpaired two-tailed *t*-test, with a significance level set at * $p < 0.01$.

The results of the in vivo investigation revealed that the blossom extract of *Zinnia elegans* L. exhibited the highest antioxidant activity (71.60%). The leaf extract demonstrated a slightly lower inhibition activity of 65.12%, and the stem extract exhibited the lowest antioxidant activity at 30.08%. The DPPH radical scavenging activity results are

consistent with those reported in the literature [9], which indicated that the ethanolic extract of *Zinnia elegans* L. leaves significantly scavenged the DPPH radicals.

The antioxidant activity of *Zinnia elegans* L. plant extracts was evaluated by ferric ion reducing antioxidant power (FRAP) assay [42,43].

As seen from the results in Figure 3, the callus culture extracts from leaves, stems, and roots of *Zinnia elegans* L. exhibited significant antioxidant activity (12.41 μmol/L, 13.99 μmol/L, and 12.55 μmol/L, respectively), which was much higher than that of plant extracts in vivo. Among these samples, blossom extract in vivo exhibited the highest antioxidant activity (6.20 μmol/L), while the stem extract exhibited the lowest (2.41 μmol/L).

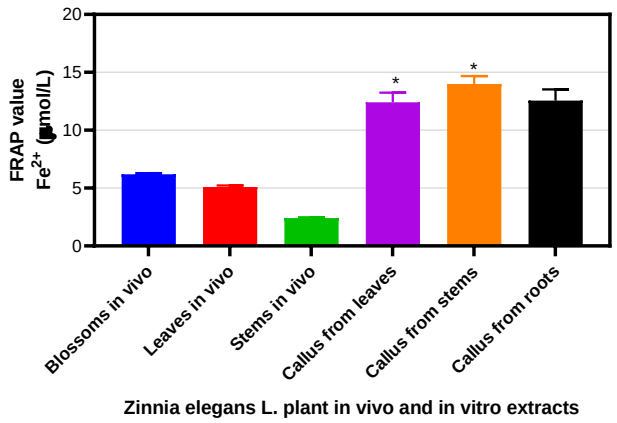

Figure 3. Antioxidative activity according to the FRAP method in *Zinnia elegans* L. plant extracts. The error bars show the mean ± SD from three replicates. Asterisks show statistically significant comparisons between *Zinnia elegans* L. plant in vivo extracts (from leaves and stems) and callus cultures (from leaves and stems) in vitro were tested with an unpaired two-tailed *t*-test, with a significance level set at * $p < 0.01$.

In summary, in the FRAP assay, the antioxidant activity (13.99 μmol/L) of the stem callus was the most significant.

3.1.2. Estimation of the Total Concentration of Phenolic Compounds

Total phenolic concentration is defined as the total amount of phenolic compounds present in a sample. The Folin–Ciocalteu assay is a common method for determining total phenolic content [42,43]. In this assay, the obtained samples formed a blue complex, the absorbance of which was measured at 725 nm.

As shown in Figure 4, the concentrations of phenolic compounds in *Zinnia elegans* L. leaf, stem, and root callus culture extracts were 27.78, 25.80, and 30.14 mg/100 g, respectively. The highest concentration was recorded in root callus extracts. The highest concentration of phenolic compounds in *Zinnia elegans* L. blossom extracts in vivo was 20.29 mg/100 mg. A slightly lower concentration of phenolic compounds was found in *Zinnia elegans* L. leaf extracts at 17.49 mg/100 mg. The stem extract of *Zinnia elegans* L. had the lowest concentration of phenolic compounds at 2.43 mg/100 mg. The high levels of phenolic and flavonoid compounds in *Zinnia elegans* L. contribute significantly to its antioxidant properties [9].

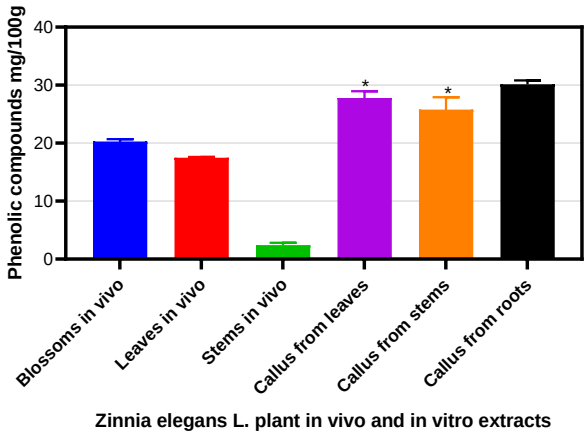

Figure 4. Concentration of phenolic compounds in plant extracts of *Zinnia elegans* L. The error bars show the mean ± SD from three replicates. Asterisks show statistically significant comparisons between *Zinnia elegans* L. plant in vivo extracts (from leaves and stems) and callus cultures (from leaves and stems) in vitro were tested with an unpaired two-tailed *t*-test, with a significance level set at * $p < 0.01$.

3.1.3. Estimation of the Concentration of Phenolic Acids

Phenolic acids are a significant class of non-flavonoid phytochemicals. They exist in both free and bound forms. A substantial body of research has demonstrated that phenols, phenolic acids, and polyphenolic compounds—including flavonoids—exhibit remarkable antioxidant features. These biochemicals play a pivotal role in neutralizing free radicals and reducing oxidative stress [10,11,28].

The phenolic acid concentration assay, according to caffeic acid, revealed that the blossom extract of *Zinnia elegans* L. exhibited the highest concentration at 2.29% (Figure 5). Concentrations in the callus cultures obtained from the leaves, stems, and roots were 1.37%, 1.49%, and 1.63%, respectively.

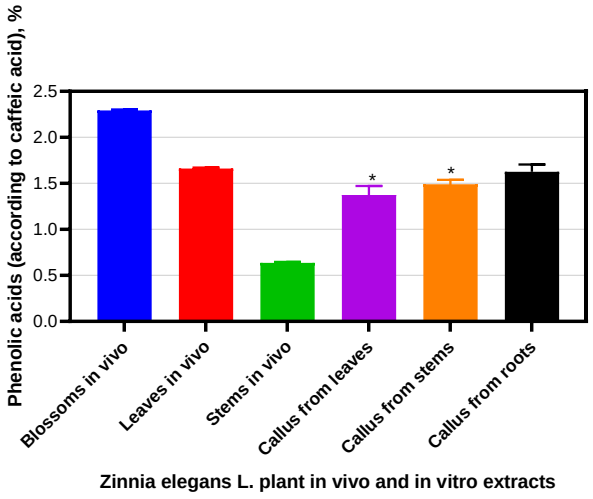

Figure 5. Phenolic acid concentration in plant extracts of *Zinnia elegans* L. The error bars show the mean ± SD from three replicates. Asterisks show statistically significant comparisons between *Zinnia elegans* L. plant in vivo extracts (from leaves and stems) and callus cultures (from leaves and stems) in vitro were tested with an unpaired two-tailed *t*-test, with a significance level set at * $p < 0.01$.

The concentration of phenolic acids in the leaf extract of *Zinnia elegans* L. was 1.66%, while the lowest concentration (0.637%) was found in the stem extract.

3.1.4. Estimation of the Total Concentration of Flavonoids

Flavonoids are a diverse group of secondary plant metabolites that play important biological roles [44]. The total flavonoid content is commonly determined using the aluminum chloride ($AlCl_3$) colorimetric assay. As shown in Figure 6, the concentration of flavonoids extracted from different parts of *Zinnia elegans* L., according to quercetin, ranged from 0.026 to 0.189 mg/g.

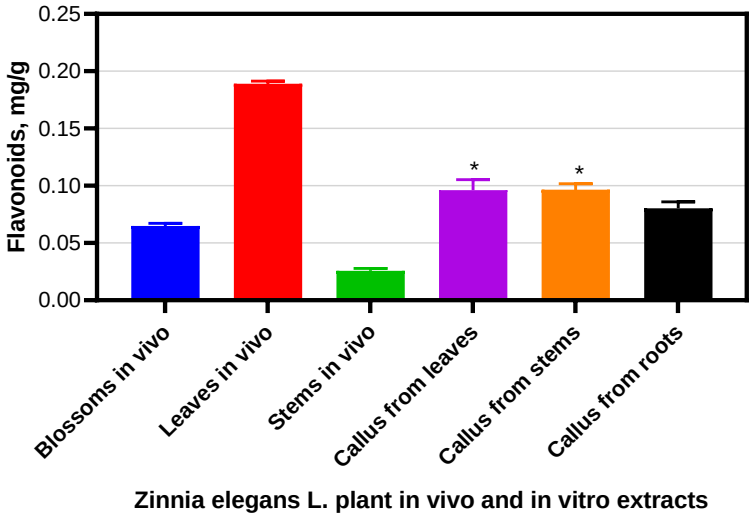

Figure 6. Flavonoid concentration (according to quercetin) in *Zinnia elegans* L. plant extracts. The error bars show the mean ± SD from three replicates. Asterisks show statistically significant comparisons between *Zinnia elegans* L. plant in vivo extracts (from leaves and stems) and callus cultures (from leaves and stems) in vitro were tested with an unpaired two-tailed *t*-test, with a significance level set at * $p < 0.01$.

The flavonoid concentration assay revealed that the leaf extract of *Zinnia elegans* L. had the highest concentration of flavonoids (according to quercetin) at 0.189 mg/g (Figure 6). The blossom extract had a lower concentration of 0.065 mg/g. The lowest concentration (0.026 mg/g) was found in the stem extract. Flavonoid concentrations of 0.096, 0.097, and 0.08 mg/g were measured in the callus culture extracts from the leaves, stems, and roots, respectively.

3.1.5. Determination of the Antibacterial Activity of *Zinnia elegans* L. Plant Extracts

The antibacterial activity of *Zinnia elegans* L. blossom, leaf, and stem extracts was determined using the agar diffusion method against chosen bacteria.

As shown in Figure 7, the extracts of *Zinnia elegans* L. blossoms and the callus cultures of the stems exhibited the highest antibacterial activity against *E. coli* with inhibition zones of 1.45 cm and 1.41 cm, respectively.

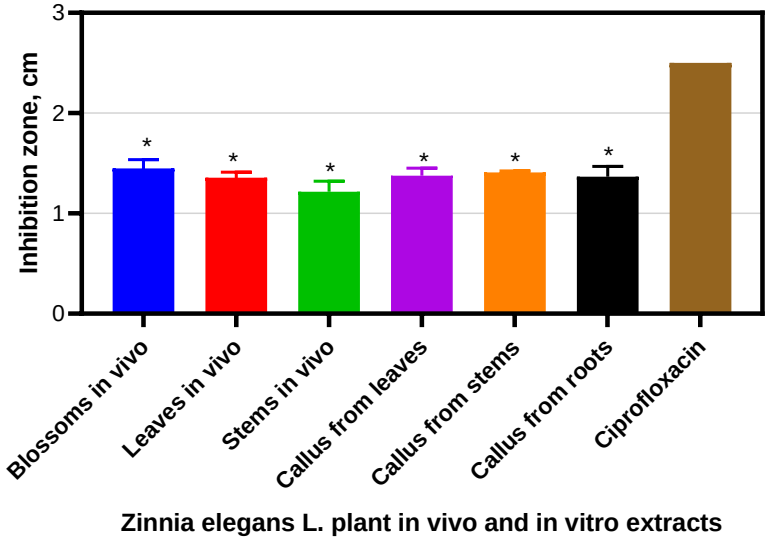

Figure 7. Antibacterial activity of *Zinnia elegans* L. against *E. coli*. The error bars show the mean ± SD from three replicates. Asterisks show statistically significant comparisons between the ciprofloxacin and plant in vivo and in vitro extract experiments, which were tested with an unpaired two-tailed *t*-test, with a significance level set at * $p < 0.01$.

Extracts from *Zinnia elegans* L. leaves in vivo (inhibition zone—1.44 cm) and callus cultures from roots (inhibition zone—1.43 cm) exhibited the highest activity against *B. subtilis* (Figure 8).

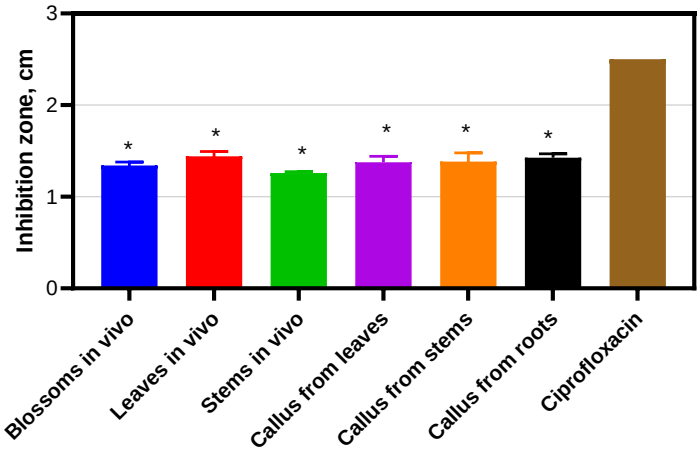

Figure 8. Antibacterial activity of *Zinnia elegans* L. against *B. subtilis*. The error bars show the mean ± SD from three replicates. Asterisks show statistically significant comparisons between the ciprofloxacin and plant in vivo and in vitro extract experiments, which were tested with an unpaired two-tailed *t*-test, with a significance level set at * $p < 0.01$.

All *Zinnia elegans* L. extracts exhibited antibacterial activity against both Gram-positive and Gram-negative pathogenic bacteria. Previous studies have also reported the antibacterial activity of *Zinnia elegans* L. against *E. coli*, *B. subtilis*, and *Staphylococcus aureus* [5]. However, both hot and cold aqueous and ethanolic extracts from *Zinnia elegans* L. leaves, stems, and blossoms showed no antibacterial activity against *Mycobacterium*

tuberculosis despite the assumption that certain plant-derived compounds might exhibit specific activity against the tubercle bacillus [7,45].

3.2. Biosynthesis of AgNPs Using Zinnia elegans L. Plant Extracts

Plant extracts from *Zinnia elegans* L., containing phytoactive metabolites, were used to synthesize AgNPs. These bioactive compounds act as reducing substances during the biosynthesis of AgNPs, enabling them to reduce Ag^+ ions into metallic Ag^0 nanoparticles.

In vivo and in vitro *Zinnia elegans* L. extracts were used for biological evaluation to comprehensively assess their biological activity. However, the AgNPs were synthesized exclusively for in vivo applications, for which biocompatibility and efficacy are paramount.

The initial reduction efficiency of $AgNO_3$ by *Zinnia elegans* L. was visually evaluated by observing a color change of the reaction mixture from yellow to dark brown. This color change is a result of the surface plasmon resonance properties of the formed AgNPs. The appearance of the brown color confirmed that Ag^+ had been successfully reduced to Ag^0 in the aqueous solution [6,8].

To optimize the yield of AgNPs, two ratios of extract to $AgNO_3$ were tested: 1:2 and 2:1. The highest yield, 0.1834 g of AgNPs, was obtained using the blossom extract at a ratio of 2:1, compared to 0.0542 g at a ratio of 1:2. A similar trend was observed with the leaf extract: 0.1724 g at a ratio of 2:1 compared to 0.0426 g at a ratio of 1:2. However, the stem extract produced AgNPs at a higher yield at a ratio of 1:2 (0.299 g) than at a ratio of 2:1 (0.0969 g). Based on these results, the 2:1 ratio using blossom extract was selected for further AgNPs analysis and characterization due to its superior yield of nanoparticles.

In summary, while protein-templated and enzyme-mediated syntheses, as well as cell-free protein bionanofactories, indeed represent promising aqueous and low-temperature routes with advantages such as narrower particle size distribution, plant-based synthesis still offers notable benefits. These include economic feasibility, environmental safety, enhanced stability and efficiency of the nanoparticles, faster biosynthesis, and reduced energy requirements [46].

3.3. Characterization of AgNPs

3.3.1. UV-Vis Absorption Spectroscopy

Ultraviolet–visible spectrophotometry is a widely used approach for analyzing nanoparticles by measuring their light absorption. This method is particularly useful for identifying metal nanoparticles through their surface plasmon resonance bands, which depend on the particle size, shape, and composition. Localized surface plasmon resonances (LSPR) arise from the coherent oscillation of conduction band electrons induced by incident light at the nanoparticle surface. For AgNPs, this phenomenon typically produces an absorption maximum within the 400–450 nm range. The peak position is highly sensitive to particle size, shape, surface state, and interparticle interactions [47]. The recorded absorption spectrum showed a distinct localized surface plasmon resonance peak centered at 462 nm, accompanied by significant spectral broadening (Figure 9).

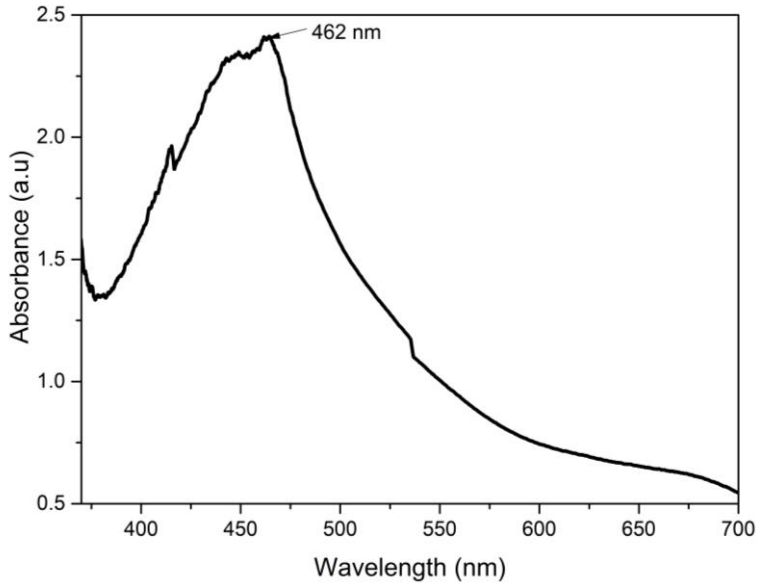

Figure 9. UV–Vis absorption spectrum of the AgNPs synthesized by the extract of the *Zinnia elegans* L. blossoms.

Such broadening is characteristic of polydisperse nanoparticle systems in which different particle sizes result in a convolution of plasmonic responses across a range of wavelengths. The absorption maximum observed at 462 nm slightly exceeds the typical range for monodisperse spherical AgNPs, indicating a red shift. This shift may be due to an increased average particle size, slight morphological anisotropy, or interparticle coupling effects caused by partial aggregation. Additionally, the broad spectral profile supports the presence of a polydisperse colloidal distribution. The position and shape of the LSPR band align well with previously reported spectra of synthesized AgNPs under similar colloidal conditions [6,19], confirming the successful formation of plasmonically active nanostructures.

3.3.2. ATR-FTIR Spectrum Analysis

Fourier transform infrared spectroscopy was used to identify the functional groups present on the surface of AgNPs synthesized using *Zinnia elegans* L. blossom extract (Figure 10). Several distinct absorption bands, which indicate the involvement of various phytochemical constituents in reducing and stabilizing the AgNPs, are seen in the ATR-FTIR spectrum.

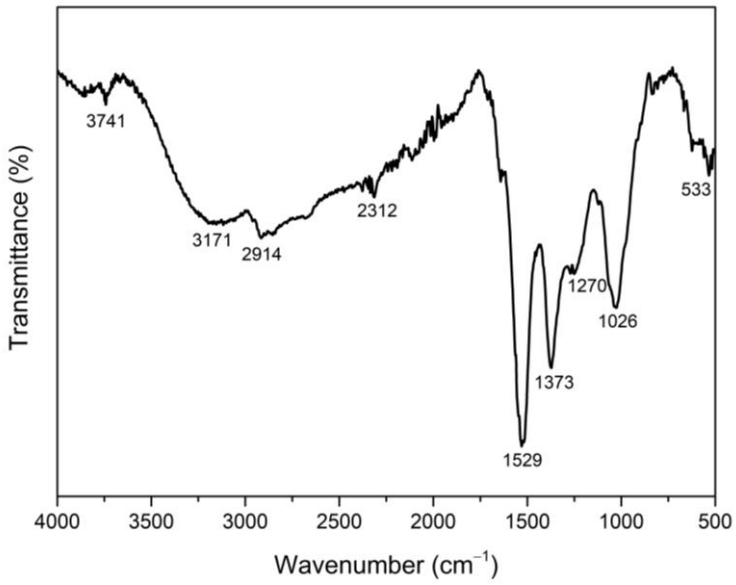

Figure 10. ATR-FTIR spectrum of AgNPs synthesized by the extract of the *Zinnia elegans* L. blossoms.

A broad band at approximately 3741 cm^{-1} corresponds to N–H amide [48] stretching, while a band at 3171 cm^{-1} corresponds to O–H stretching vibrations that are typically associated with the hydroxyl groups in phenols, alcohols, or flavonoids [49,50]. The band at 2914 cm^{-1} has been assigned to C–H stretching vibrations of aliphatic –CH_2 groups, suggesting the presence of long-chain hydrocarbons or terpenoids. The absorption band at 2312 cm^{-1} can be attributed to stretching vibrations of C≡C or possibly interactions of CO_2 absorbed from the atmosphere. The intensive band at 1529 cm^{-1} may correspond to the asymmetric N–O stretching (possibly in nitro compounds) or aromatic C=C stretching in polyphenolic compounds. The peak at 1373 cm^{-1} is characteristic of C–N stretching vibrations, indicating the presence of amine groups. The bands at 1270 cm^{-1} and 1026 cm^{-1} are commonly associated with C–O stretching vibrations, probably from alcohols, esters, or ethers. Notably, an absorption peak at 533 cm^{-1} corresponds to Ag–Ag bond vibrations, confirming interaction between the silver core and biomolecules in the extract. This indicates successful capping and stabilization of AgNPs by plant-derived compounds [50,51]. The broad stretching vibrations corresponding to the H–C=O, i.e., C–H functional groups of aldehydes and the –OH groups of alcohols and phenols, indicate that the biomolecules in the extract can act as reducing, capping, and stabilizing agents in the synthesis of AgNPs [8,40,50]. The *Zinnia elegans* L. plant extract contains various polyphenolic compounds that can chelate silver ions and subsequently reduce them to zero-valent AgNPs.

3.3.3. X-ray Diffraction Analysis

The crystalline structure and average crystallite size of the synthesized AgNPs were investigated using X-ray diffraction. The diffraction pattern revealed characteristic peaks at 2θ values of 38.13°, 44.33°, and 64.51°, as seen in Figure 11. These peaks correspond to the (111), (200), and (220) crystallographic planes of the face-centered cubic (FCC) silver structure, respectively. The presence of these peaks confirms the crystalline nature of the AgNPs and their FCC structure, which is consistent with the standard JCPDS card No. 04-0783 [38,50,52,53]. Additional peaks also appear in the diffractogram at 2θ = 27.74°, 32.09°, 34.34°, 46.17°, 48.11°, and 53.88°, 57.43° (marked with stars) and are weaker than the silver peaks. These spectral peaks are ascribed to the presence of crystallized organic compounds acting as capping and stabilizing agents on the surface of the AgNPs. Comparable

findings have been documented for AgNPs synthesized via eco-friendly synthesis methods [49,50,54].

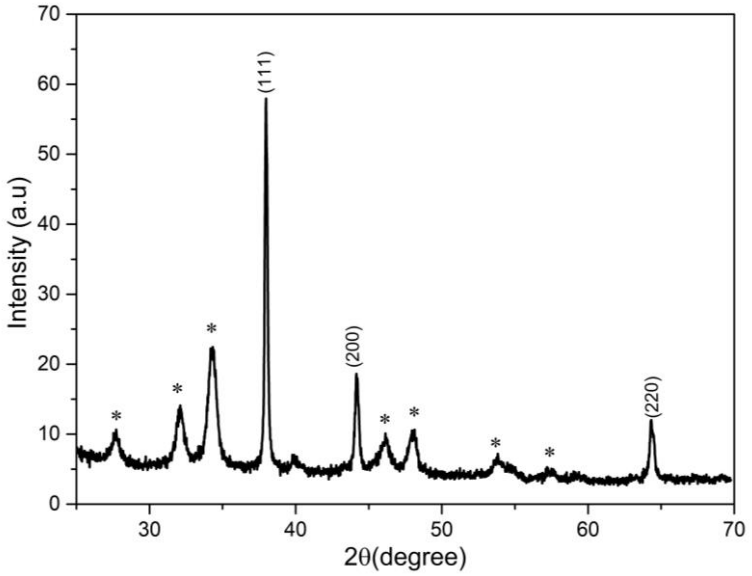

Figure 11. The diffractogram of AgNPs synthesized using the extract of *Zinnia elegans* L. blossoms. *– Crystallized organic compounds.

The average crystallite size of the Ag nanoparticles was determined using the Debye–Scherrer equation [36] and yielded a value of approximately 25 nm. The crystalline size of the AgNPs varies depending on the synthesis method and the biological reducing agents used. Reported sizes range from 5.5 nm [55] to approximately 60 nm [6,48]. Other studies report sizes within the 10–30 nm range [38,56].

The experimental values of *d* (lattice spacing) for the crystallites and the lattice parameters (*a*) of AgNP crystallites are shown in Table 1.

Table 1. Data on the crystallite diameter size (*D*), full width at half maximum (*FWHM, β*), interplanar spacing (*d*), and lattice parameters (*a*) of the prepared AgNPs.

2θ of the Intense Peak (°)	***FWHM*** β_{hkl} **(°)**	**Miller Indices (*hkl*)**	**Crystallite Diameter *D* (nm)**	**Interplanar Spacing *d* (nm)**	**Lattice Parameters *a* (nm)**
38.13	0.229	111	36.70	0.236	0.4085
44.33	0.405	200	21.19	0.204	0.4084
64.51	0.507	220	18.54	0.144	0.4082
Average values (nm)			25.48	0.195	0.4084

The experimentally determined average lattice parameter (0.4084 nm) closely matches the standard value for FCC silver, as reported in JCPDS card No. 04-0783 (a = 0.4086 nm) [38], thereby confirming the crystalline nature and phase purity of the synthesized nanoparticles.

3.3.4. SEM/EDX Analysis of AgNPs

SEM was applied to examine the surface morphology of the AgNPs produced using *Zinnia elegans* L. blossom extract. The representative micrograph is presented in Figure 12. The nanoparticles exhibited predominantly spherical morphology with moderate polydispersity. Some aggregation was observed, which is commonly associated with the high surface energy of nanoscale materials and the partial capping of biomolecules in the

plant extract. The relatively smooth surfaces and visible particle boundaries confirm the particles' nanoscale dimensions.

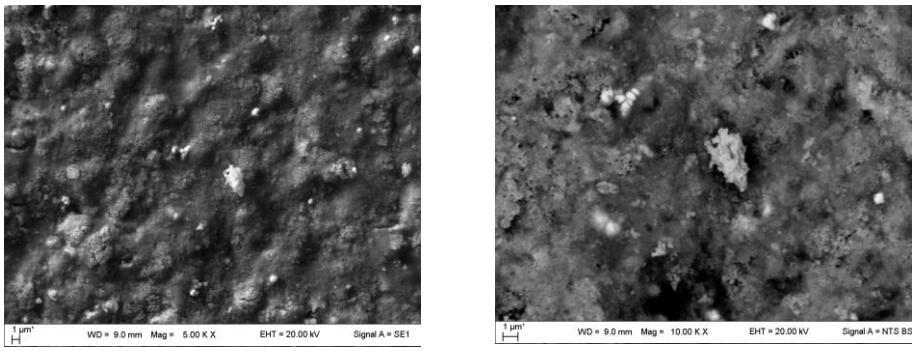

(**a**) (**b**)

Figure 12. SEM images of AgNPs synthesized by the extract of the *Zinnia elegans* L. blossoms: (**a**) ×5000; (**b**) ×10,000.

EDX analysis was performed to determine the sample's elemental composition (Figure S1). The EDS spectrum revealed a strong peak corresponding to metallic silver, thereby confirming the successful synthesis of AgNPs. Quantitative analysis of the sample (Table S1) revealed that silver was present in the highest quantity (84.74 at.%), while minor amounts of carbon (4.57 at.%), oxygen (7.67 at.%), and chlorine (3.02 at.%) were also detected. The presence of carbon and oxygen can be attributed to organic compounds derived from the *Zinnia elegans* L. extract that likely acted as reducing and capping agents during biosynthesis. The presence of chlorine may be attributed to metabolites or precursors from the residual plants used in the synthesis process. The high silver content, in conjunction with the absence of other metallic impurities, indicates the purity of the obtained AgNPs and efficacy of the green synthesis method.

3.3.5. TEM/EDX Analysis of AgNPs

TEM analysis was carried out to explore the morphology and size distribution of AgNPs biosynthesized using the blossom extract of *Zinnia elegans* L. Figures 13 and S2 show that the AgNPs were predominantly spherical and relatively uniform in shape, though some variation in size was observed. While the particles are well dispersed, they tend to form small agglomerates due to interparticle interactions and the presence of residual phytochemicals from the *Zinnia elegans* L. extract.

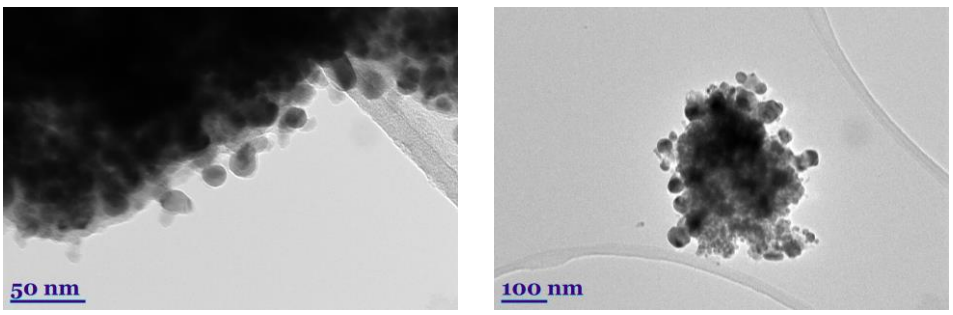

(**a**) (**b**)

Figure 13. TEM images of AgNPs synthesized by the extract of the *Zinnia elegans* L. blossoms: (**a**) 50 nm; (**b**) 100 nm.

The image confirmed that the particles were in the nanometer range, with the majority of the particles being less than 50 nm in diameter. Some larger particles or aggregates were also visible, possibly resulting from partial coalescence during synthesis or drying. The high-resolution contrast indicates that the nanoparticles are crystalline in nature, which is consistent with the SEM and XRD results. The TEM analysis results were correlated with those of the XRD results, which reported an average crystallite size of around 25 nm for the AgNPs. According to the literature [38,56], the surface plasmon of nanoparticles with such diameters and spherical shapes is usually detected at 450–470 nm. Thus, these results also correlate with the ones of UV–Vis analysis.

The EDX spectrum confirms the presence of elemental silver, thereby supporting the findings obtained from the XRD analysis (Figure S3).

3.3.6. TGA/DTA Analysis of AgNPs

TGA/DTA were performed on biosynthesized AgNPs over a temperature range of 30–930 °C (Figure 14). These analyses evaluated the thermal resistance of biosynthesized nanoparticles and identified the presence of oxygen-containing functional groups. The thermogram showed continuous weight loss in four stages. The first stage accounted for approximately 3% weight loss between room temperature and 165 °C and was due to the evaporation of physically adsorbed water and other volatile impurities. The second phase, observed between 165 °C and 265 °C, exhibited a 13% mass decrease, likely resulting from the thermal decomposition of surface-bound organic stabilizers, including reducing sugars and carbonyl-containing capping agents. These findings are consistent with the ATR-FTIR results (Figure 10), which confirm the presence of such functional groups on the nanoparticle surface. Further degradation occurred in the third (265–560 °C) and fourth (560–900 °C) phases, producing additional mass losses of 16% and 8%, respectively. These stages were likely linked to the continued breakdown of organic components and structural alterations of the AgNPs at higher temperatures. Based on the total mass loss profile, it can be inferred that the sample was approximately 59.81% pure, thermally stable elemental silver. These data confirm the high silver content and thermal stability of the synthesized nanoparticles. These findings are consistent with the previous reports on the biosynthesis of AgNPs, which also demonstrated comparable levels of purity [53,57].

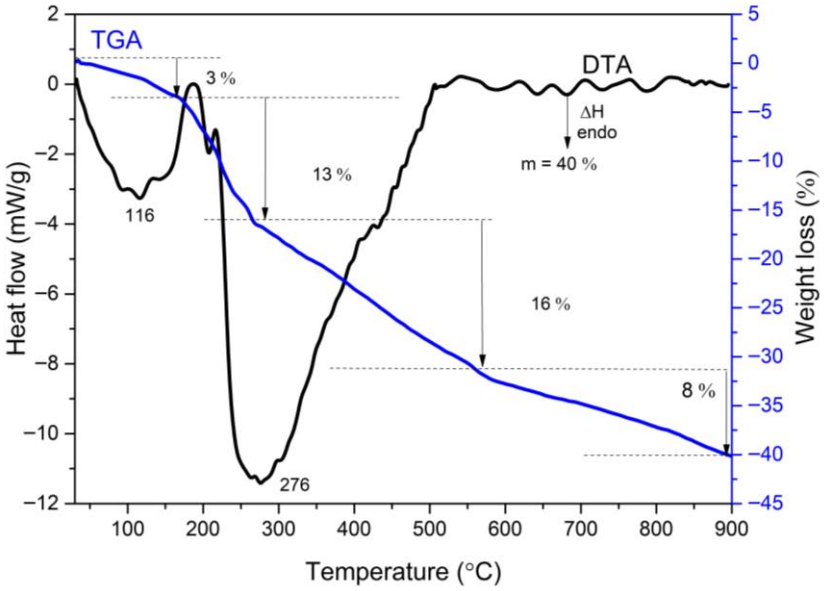

Figure 14. TGA/DTA thermogram of AgNPs synthesized by the extract of the *Zinnia elegans* L. blossoms.

The corresponding DTA curve showed two prominent endothermic peaks. The first peak, which was observed at 116 °C, was likely associated with the evaporation of adsorbed water or other physically bound species. The second, intense endothermic peak, detected at 276 °C, was presumed to be associated with crystallization processes of AgNPs [58].

3.4. Antibacterial Activity of AgNPs

The antibacterial assay of AgNPs was performed by testing their properties against *E. coli* and *B. subtilis* bacteria. The antibiotic ciprofloxacin was used as a positive control. AgNPs act on bacterial strains through two pathways: action at the bacterial cell membrane level and alteration of the bacterial cellular content. AgNPs can bind to the bacterial cell membrane, causing damage and increased permeability. Ultimately, this leads to cell death due to leakage of cellular material. AgNPs have been reported to directly affect cellular mechanisms within bacteria by altering the structure and function of their DNA and proteins [6,24,59].

3.4.1. Antibacterial Activity of AgNPs Against *E. coli*

Antibacterial activity assays using colloidal solutions of AgNPs synthesized with *Zinnia elegans* L. blossom, leaf, and stem extracts revealed that those synthesized with blossom extract exhibited the strongest antibacterial effect against *E. coli*, with an inhibition zone diameter of 2.27 cm (Figures 15 and 16). Those synthesized using leaf and stem extracts showed slightly lower activity, with inhibition zones measuring 1.96 cm and 1.93 cm, respectively. Comparing the antibacterial activity of the blossom-derived AgNPs with that of the antibiotic ciprofloxacin demonstrated that the AgNPs were similarly effective against *E. coli*, indicating their strong antibacterial potential.

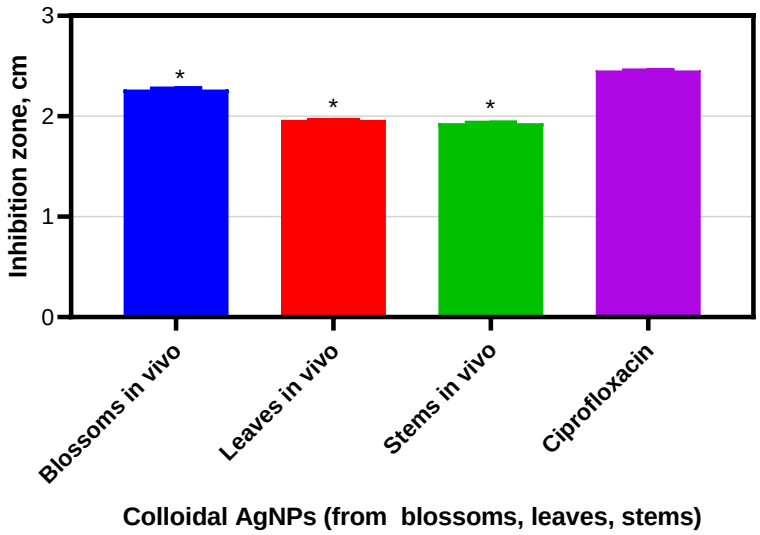

Figure 15. Antibacterial activity of colloidal AgNPs (from blossoms, leaves, and stems) against *E. coli*. The error bars show the mean ± SD from three replicates. Asterisks show statistically significant comparisons between the ciprofloxacin and plant in vivo extract experiments, which were tested with an unpaired two-tailed *t*-test, with a significance level set at * $p < 0.01$.

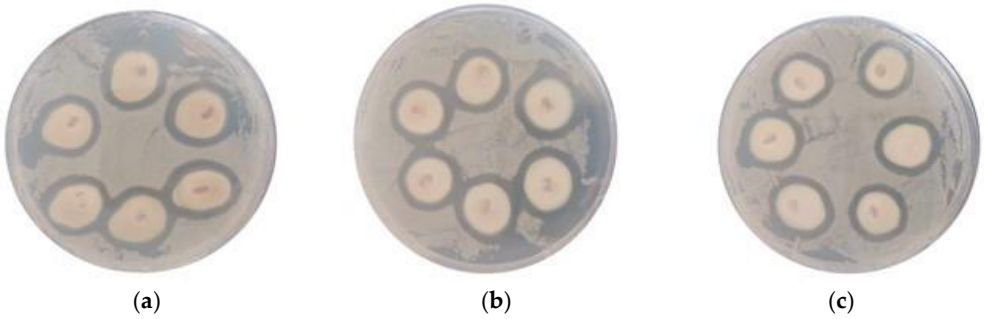

(**a**) (**b**) (**c**)

Figure 16. Inhibition zones formed by colloidal AgNPs synthesized using *Zinnia elegans* L. extracts against *E. coli*: (**a**) blossoms; (**b**) leaves; (**c**) stems.

3.4.2. Antibacterial Activity of AgNPs Against *B. subtilis*

Assays of antibacterial activity using colloidal solutions of AgNPs synthesized using *Zinnia elegans* L. blossom, leaf, and stem extracts revealed that those synthesized with blossom extract exhibited the strongest antibacterial activity against the Gram-positive bacterium *B. subtilis*, with respective inhibition zone diameters of 2.31 cm and 2.27 cm, respectively (Figures 17 and 18). Colloidal AgNPs synthesized with stem extract exhibited slightly lower activity, with an inhibition zone diameter of 2.10 cm. It is worth noting that the antibacterial test of colloidal AgNPs synthesized with blossom and leaf extracts against *B. subtilis* is on par with that of ciprofloxacin and, thus, reveals a promising potential of nanoparticles synthesized using an eco-friendly green synthesis pathway.

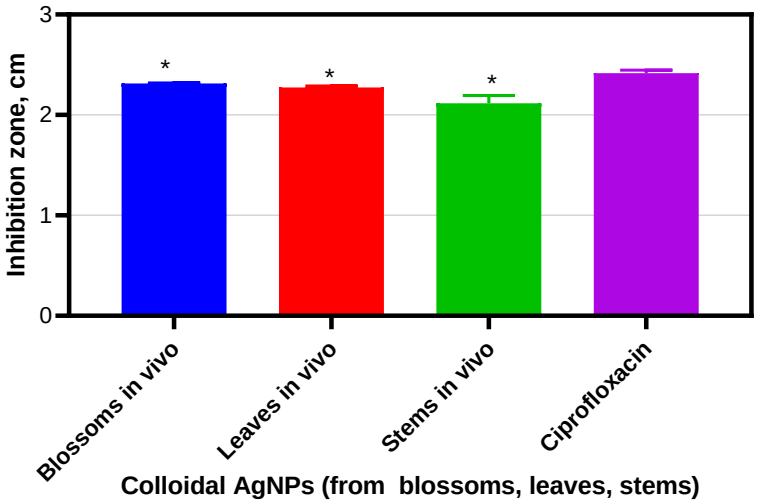

Figure 17. Antibacterial activity of colloidal AgNPs solutions (from blossoms, leaves, and stems) against *B. subtilis.* The error bars show the mean ± SD from three replicates. Asterisks show statistically significant comparisons between the ciprofloxacin and plant in vivo extracts experiments, which were tested with an unpaired two-tailed *t*-test, with a significance level set at * $p < 0.01$.

(**a**) (**b**) (**c**)

Figure 18. Inhibition zones formed by colloidal AgNPs synthesized using *Zinnia elegans* L. extracts against *B. subtilis*: (**a**) blossoms; (**b**) leaves; (**c**) stems.

Essentially, it is critical to explore the long-term impact of using AgNPs on microbial communities and the development of resistance. This could involve examining the environmental fate of AgNPs, conducting green toxicological tests, and investigating their environmental impact [60].

4. Conclusions

This study has shown that extracts from *Zinnia elegans* L. have substantial antioxidant and antibacterial properties. These properties are primarily due to the plant's high phenolic compound content, including phenolic acids and flavonoids. The antioxidant capacity of *Zinnia elegans* L. extracts was evaluated through different bioassays, which demonstrated that callus culture extracts exhibited the highest levels of antioxidant activity. *Zinnia elegans* L. demonstrates significant potential for synthesizing bioactive phytometabolites through in vitro callus cultures. This enhanced capacity can be linked to the elevated concentrations of bioactive phenolic compounds, which are known to scavenge free radicals and mitigate oxidative stress. In addition to their antioxidant properties, extracts from *Zinnia elegans* L. exhibit significant antibacterial activity against selected microbial pathogens.

The research provides a thorough examination of the plant's biosynthesis of AgNPs utilizing extracts from *Zinnia elegans* L., showcasing the remarkable potential of this plant in nanotechnology applications. Formation of the AgNPs was confirmed by a color change of the reaction mixture, a characteristic UV–Vis absorption peak at 462 nm, and results of EDX analysis. ATR-FTIR data supported the involvement of phenolic compounds in the reduction and stabilization processes. XRD analysis of AgNPs revealed an average crystallite size of approximately 25 nm. This is consistent with TEM observations showing the AgNPs to be spherical, with an average particle size below 50 nm. The XRD pattern also confirmed the face-centered cubic crystalline structure of the silver with a lattice constant of 0.4084 nm. Complementary TGA/DTA analysis revealed a total mass loss of 40%, indicating that the biosynthesized nanoparticles contain approximately 60% pure elemental silver. The AgNPs exhibited pronounced antibacterial activity against the selected bacteria, indicating their potential applicability in industrial biotechnology.

This study highlights the successful biosynthesis of AgNPs using *Zinnia elegans* L. extracts, emphasizing the plant's potential as a valuable resource for sustainable, advanced nanobiotechnology applications. The possible uses of enzyme immobilization highlight the significance of this research, suggesting that the integration of biogenic nanoparticles could revolutionize various industrial processes. As we move towards a more sustainable future, the findings of this study serve as a testament to the innovative possibilities that nature offers in the development of advanced nanomaterials. Future investigations should further explore the functional properties of these plant-synthesized AgNPs

and their applications in diverse fields, ultimately contributing to a greener and more efficient technological landscape. Continued research in this field will elucidate the mechanisms of nanoparticle formation and expand their applications in medicine, agriculture, and environmental science.

In conclusion, although AgNPs demonstrate significant biopharmaceutical applications, their potential risks to biological systems highlight the need for further studies on their biocompatibility and green toxicology. Integrating safer design concepts and performing comprehensive safety assessments are essential for ensuring their responsible use across various fields. Additionally, future research should focus on developing safer photodynamic therapeutic agents using plant-mediated AgNPs synthesized via microemulsions. Green synthesis methods represent a promising approach to the sustainable and eco-friendly production of nanoparticles, consistent with the principles of advanced biotechnology and engineering. Further investigations in this field will contribute to overcoming current challenges and fully realizing the prospects of green nanotechnology.

Supplementary Materials: The following supporting information can be downloaded at: https://www.mdpi.com/article/doi/s1, Figure S1: EDX spectrum of AgNPs formed using *Zinnia elegans* L. blossom extract (by SEM analysis); Table S1: EDX data; Figure S2: TEM of AgNPs formed using *Zinnia elegans* L. blossom extract; Figure S3: EDX spectrum of AgNPs formed using *Zinnia elegans* L. blossom extract (by TEM analysis).

Author Contributions: Conceptualization, I.J., J.N., K.K., I.T., R.S. and N.P.; methodology, I.J., J.N., K.K., I.T., R.S. and N.P.; software, I.J. and N.P.; validation, I.J., J.N., K.K., I.T. and N.P.; formal analysis, I.J., J.N., K.K., I.T., R.S. and N.P.; investigation, I.J., J.N., K.K., I.T., R.S. and N.P.; resources, I.J., J.N., K.K., I.T., R.S. and N.P.; data curation, I.J., J.N., K.K., I.T., R.S. and N.P.; writing—original draft preparation, I.J., J.N., K.K., I.T., R.S. and N.P.; writing—review and editing, I.J., J.N., K.K., I.T., R.S. and N.P.; visualization, I.J., J.N., K.K., I.T., R.S. and N.P.; supervision, I.J., J.N., K.K., I.T. and N.P. All authors have read and agreed to the published version of the manuscript.

Funding: This research received no external funding.

Institutional Review Board Statement: The *Zinnia elegans* L. seeds were purchased from UAB Agrofirma "Sėklos“ in Lithuania. Callus cultures were established from these seeds in the Biotechnology Laboratory at the Department of Organic Chemistry, Faculty of Chemical Technology at Kaunas University of Technology, using Murashige and Skoog (MS) medium supplemented with 6-benzylaminopurine (BAP) (1 mg/L) and 1-naphtylacetic acid (NAA) (1 mg/L). The callus culture cycle was maintained for 30 days under controlled conditions in the laboratory.

Informed Consent Statement: Not applicable.

Data Availability Statement: The original contributions presented in this study are included in the article. Further inquiries can be directed to the corresponding author.

Conflicts of Interest: The authors declare no conflicts of interest.

Abbreviations

The following abbreviations are used in this manuscript:

AgNPs	Silver nanoparticles
BAP	6-Benzylaminopurine
NAA	1-Nahtylacetic acid
DPPH	2,2-Diphenyl-1-picrylhydrazyl
FRAP	Ferric ion reducing antioxidant power
XRD	X-ray diffraction
FCC	Face-centered cubic

FTIR	Fourier transform infrared
SEM	Scanning electron microscopy
TEM	Transmission electron microscopy
EDX	Energy-dispersive X-ray spectroscopy
TGA	Thermogravimetric analysis
DTA	Differential thermal analysis

References

1. Souza, F.J.C., Jr.; Assunção, M.C. First Report of Meloidogyne Javanica Infecting Zinnia Elegans in Ceará State, Brazil. *J. Nematol.* **2020**, *52*, 1–4. https://doi.org/10.21307/jofnem-2020-066.
2. Ozturk, M.; Sagdollina, N.R.; Ibrayeva, M.M. Component Composition and Biological Activity of Essential Oil of Plant *Zinnia elegans*. *Int. J. Biol. Chem.* **2023**, *16*, 90–96. https://doi.org/10.26577/IJBCh2023v16i2a9.
3. Burlec, A.F.; Pecio, Ł.; Mircea, C.; Cioancă, O.; Corciovă, A.; Nicolescu, A.; Oleszek, W.; Hăncianu, M. Chemical Profile and Antioxidant Activity of Zinnia Elegans Jacq. Fractions. *Molecules* **2019**, *24*, 2934. https://doi.org/10.3390/molecules24162934.
4. Gomaa, A.A.-R.; Samy, M.N.; Abdelmohsen, U.R.; Krischke, M.; Mueller, M.J.; Wanas, A.S.; Desoukey, S.Y.; Kamel, M.S. Metabolomic Profiling and Anti-Infective Potential of *Zinnia elegans* and *Gazania rigens* (Family Asteraceae). *Nat. Prod. Res.* **2020**, *34*, 2612–2615. https://doi.org/10.1080/14786419.2018.1544975.
5. Tulub, I.; Burda, N. Study of antimicrobial activity of *Zinnia elegans* raw materials. *Ann. Mechnikov Inst.* **2023**, *4*, 150–153. https://doi.org/10.5281/zenodo.10255334.
6. Goonewardene, G.; Kandiah, M.; Gunaratne, B.; Perera, O. Sustainable Synthesis of Silver Nanoparticles via Zinnia Elegans Leaf Extract: A Nano Catalytic Approach in Catalysis Applications. *Int. J. Res. Innov. Appl. Sci.* **2025**, *X*, 683–702. https://doi.org/10.51584/IJRIAS.2025.10020058.
7. Gomaa, A.; Samy, M.; Desoukey, S.; Kamel, M. A Comprehensive Review of Phytoconstituents and Biological Activities of Genus Zinnia. *J. Adv. Biomed. Pharm. Sci.* **2018**, *2*, 29–37. https://doi.org/10.21608/jabps.2018.5599.1024.
8. Haque, S.; Norbert, C.C.; Acharyya, R.; Mukherjee, S.; Kathirvel, M.; Patra, C.R. Biosynthesized Silver Nanoparticles for Cancer Therapy and In Vivo Bioimaging. *Cancers* **2021**, *13*, 6114. https://doi.org/10.3390/cancers13236114.
9. Samy, M.N.; Gomaa, A.A.-R.; Attia, E.Z.; Ibrahim, M.A.A.; Desoukey, S.Y.; Kamel, M.S. Flavonoids of *Zinnia elegans*: Chemical Profile and in Vitro Antioxidant and in Silico Anti-COVID-19 Activities. *S. Afr. J. Bot.* **2022**, *147*, 576–585. https://doi.org/10.1016/j.sajb.2022.02.024.
10. Gupta, N.; Upadhyaya, C.P.; Singh, A.; Abd-Elsalam, K.A.; Prasad, R. Applications of Silver Nanoparticles in Plant Protection. In *Nanobiotechnology Applications in Plant Protection*; Abd-Elsalam, K.A., Prasad, R., Eds.; Springer International Publishing: Cham, Switzerland, 2018; pp. 247–265, ISBN 978-3-319-91161-8.
11. Mathur, P.; Jha, S.; Ramteke, S.; Jain, N.K. Pharmaceutical Aspects of Silver Nanoparticles. *Artif. Cells Nanomed. Biotechnol.* **2018**, *46*, 115–126. https://doi.org/10.1080/21691401.2017.1414825.
12. Jadhav, R.; Bhide, S.; Prasad, B.L.V.; Kunchiraman, B.; Shimpi, J.; Nandhini, U. Silver Nanoparticles: A New Perspective in Endodntic Therapy. *IIOAB J.* **2016**, *7*, 77–81.
13. Lee, S.H.; Jun, B.-H. Silver Nanoparticles: Synthesis and Application for Nanomedicine. *Int. J. Mol. Sci.* **2019**, *20*, 865. https://doi.org/10.3390/ijms20040865.
14. Chikkanayakanahalli Paramesh, C.; Giridasappa, A.; Channapillekoppalu Siddegowda, A.K.; Rangappa, D.; Doddakunche Shivaramu, P. Chapter 1—History, Introduction, and Physicochemical Properties of Silver Nanoparticles. In *Silver Nanoparticles for Drug Delivery*; Kesharwani, P., Ed.; Academic Press: Cambridge, MA, USA, 2024; pp. 1–38, ISBN 978-0-443-15343-3.
15. Seku, K.; Hussaini, S.S.; Bhagavanth Reddy, G.; Radha Krishna Reddy, M. Chapter 9—Silver-Based Biofungicides for the Suppression of Pathogenic Fungi in Agriculture Fields. In *Nanofungicides*; Abd-Elsalam, K.A., Ed.; Nanobiotechnology for Plant Protection; Elsevier: Amsterdam, The Netherlands, 2024; pp. 169–194, ISBN 978-0-323-95305-4.
16. Verma, A.; Srivastava, M. Novel Silver Nanoparticles as Modern Defense Tools in Agro-Ecosystem. In *Ecosystem Services: Types, Management, and Benefits*; Jatav, H.S., Rajput, V.D., Eds.; Series: Agriculture Issues and Policies; Nova Science Publishers, Inc.: Hauppauge, New York, NY, USA, 2022; pp. 23–44, ISBN 978-1-68507-614-6.
17. Mo, F.; Zhou, Q.; He, Y. Nano–Ag: Environmental Applications and Perspectives. *Sci. Total Environ.* **2022**, *829*, 154644. https://doi.org/10.1016/j.scitotenv.2022.154644.

18. Santhosh, A.; Theertha, V.; Prakash, P.; Smitha Chandran, S. From Waste to a Value Added Product: Green Synthesis of Silver Nanoparticles from Onion Peels Together with Its Diverse Applications. *Mater. Today Proc.* **2021**, *46*, 4460–4463. https://doi.org/10.1016/j.matpr.2020.09.680.
19. Abbasi, E.; Milani, M.; Fekri Aval, S.; Kouhi, M.; Akbarzadeh, A.; Tayefi Nasrabadi, H.; Nikasa, P.; Joo, S.W.; Hanifehpour, Y.; Nejati-Koshki, K.; et al. Silver Nanoparticles: Synthesis Methods, Bio-Applications and Properties. *Crit. Rev. Microbiol.* **2014**, *42*, 173–180. https://doi.org/10.3109/1040841X.2014.912200.
20. Prajapati, S.; Yadav, S.; Khan, J. Bionanofactories for the Environmental Friendly Fabrication of Silver Nanoparticles: Application to the Analysis of Antimicrobial Agents. *Curr. Pharm. Anal. 20*, 98–114. https://doi.org/10.2174/0115734129281373240214071815.
21. Galatage, S.T.; Hebalkar, A.S.; Gote, R.V.; Mali, O.R.; Killedar, S.G. Silver Nano Particles by Green Synthesis: An Overview. *Res. J. Pharm. Technol.* **2020**, *13*, 1503–1510. https://doi.org/10.5958/0974-360X.2020.00274.7.
22. Fahim, M.; Shahzaib, A.; Nishat, N.; Jahan, A.; Bhat, T.A.; Inam, A. Green Synthesis of Silver Nanoparticles: A Comprehensive Review of Methods, Influencing Factors, and Applications. *JCIS Open* **2024**, *16*, 100125. https://doi.org/10.1016/j.jciso.2024.100125.
23. Rodríguez-Félix, F.; Graciano-Verdugo, A.Z.; Moreno-Vásquez, M.J.; Lagarda-Díaz, I.; Barreras-Urbina, C.G.; Armenta-Villegas, L.; Olguín-Moreno, A.; Tapia-Hernández, J.A. Trends in Sustainable Green Synthesis of Silver Nanoparticles Using Agri-Food Waste Extracts and Their Applications in Health. *J. Nanomater.* **2022**. https://doi.org/10.1155/2022/8874003
24. Rajeshkumar, S.; Bharath, L.V.; Geetha, R. Broad Spectrum Antibacterial Silver Nanoparticle Green Synthesis: Characterization, and Mechanism of Action. In *Green Synthesis, Characterization and Applications of Nanoparticles*; Elsevier: Amsterdam, The Netherlands, 2019; pp. 429–444, ISBN 978-0-08-102579-6.
25. Jain, A.S.; Pawar, P.S.; Sarkar, A.; Junnuthula, V.; Dyawanapelly, S. Bionanofactories for Green Synthesis of Silver Nanoparticles: Toward Antimicrobial Applications. *Int. J. Mol. Sci.* **2021**, *22*, 11993. https://doi.org/10.3390/ijms222111993.
26. Chung, I.-M.; Park, I.; Seung-Hyun, K.; Thiruvengadam, M.; Rajakumar, G. Plant-Mediated Synthesis of Silver Nanoparticles: Their Characteristic Properties and Therapeutic Applications. *Nanoscale Res. Lett.* **2016**, *11*, 40. https://doi.org/10.1186/s11671-016-1257-4.
27. Abdellatif, A.A.H.; Mostafa, M.A.H.; Konno, H.; Younis, M.A. Exploring the Green Synthesis of Silver Nanoparticles Using Natural Extracts and Their Potential for Cancer Treatment. *3 Biotech* **2024**, *14*, 274. https://doi.org/10.1007/s13205-024-04118-z.
28. Kazlagić, A.; Abud, O.A.; Ćibo, M.; Hamidović, S.; Borovac, B.; Omanović-Mikličanin, E. Green Synthesis of Silver Nanoparticles Using Apple Extract and Its Antimicrobial Properties. *Health Technol.* **2020**, *10*, 147–150. https://doi.org/10.1007/s12553-019-00378-5.
29. Fiorati, A.; Bellingeri, A.; Punta, C.; Corsi, I.; Venditti, I. Silver Nanoparticles for Water Pollution Monitoring and Treatments: Ecosafety Challenge and Cellulose-Based Hybrids Solution. *Polymers* **2020**, *12*, 1635. https://doi.org/10.3390/polym12081635.
30. Rathi B., S.; Kumar P., S.; Senthilkumar, S.; Vellaichamy, P.; Rangasamy, G.; N. Vo, D.-V. Innovative Eco-Friendly Silver Nanoparticles: Various Synthesis Methods, Characterization and Prospective Applications. *Chem. Eng. Commun.* **2025**, *212*, 472–507. https://doi.org/10.1080/00986445.2024.2403117.
31. Jonuškienė, I.; Stankevičienė, R.; Kantminienė, K.; Tumosienė, I. The Influence of Phytohormones on Antioxidative and Antibacterial Activities in Callus Cultures of *Hypericum perforatum* L. *Agriculture* **2023**, *13*, 1543. https://doi.org/10.3390/agriculture13081543.
32. Nutautaitė, M.; Racevičiūtė-Stupelienė, A.; Bliznikas, S.; Jonuškienė, I.; Karosienė, J.; Koreivienė, J.; Vilienė, V. Evaluation of Phenolic Compounds and Pigments in Freshwater Cladophora Glomerata Biomass from Various Lithuanian Rivers as a Potential Future Raw Material for Biotechnology. *Water* **2022**, *14*, 1138. https://doi.org/10.3390/w14071138.
33. Fabrowska, J.; Messyasz, B.; Pankiewicz, R.; Wilińska, P.; Łęska, B. Seasonal Differences in the Content of Phenols and Pigments in Thalli of Freshwater *Cladophora glomerata* and Its Habitat. *Water Res.* **2018**, *135*, 66–74. https://doi.org/10.1016/j.watres.2018.02.020.
34. Kvasnička, F.; Čopíková, J.; Ševčík, R.; Krátká, J.; Syntytsia, A.; Voldřich, M. Determination of Phenolic Acids by Capillary Zone Electrophoresis and HPLC. *Cent. Eur. J. Chem.* **2008**, *6*, 410–418. https://doi.org/10.2478/s11532-008-0032-5.
35. Khuluk, R.H.; Yunita, A.; Rohaeti, E.; Syafitri, U.D.; Linda, R.; Lim, L.W.; Takeuchi, T.; Rafi, M. An HPLC-DAD Method to Quantify Flavonoids in Sonchus Arvensis and Able to Classify the Plant Parts and Their Geographical Area through Principal Component Analysis. *Separations* **2021**, *8*, 12. https://doi.org/10.3390/separations8020012.
36. Patterson, A.L. The Scherrer Formula for X-Ray Particle Size Determination. *Phys. Rev.* **1939**, *56*, 978–982. https://doi.org/10.1103/PhysRev.56.978.

37. Bragg, W.H.; Bragg, W.L. The Reflection of X-rays by Crystals. *Proc. R. Soc. Lond. Ser. Contain. Pap. Math. Phys. Character* **1997**, *88*, 428–438. https://doi.org/10.1098/rspa.1913.0040.
38. Ali, Md.H.; Azad, Md.A.K.; Khan, K.A.; Rahman, Md.O.; Chakma, U.; Kumer, A. Analysis of Crystallographic Structures and Properties of Silver Nanoparticles Synthesized Using PKL Extract and Nanoscale Characterization Techniques. *ACS Omega* **2023**, *8*, 28133–28142. https://doi.org/10.1021/acsomega.3c01261.
39. Kainz, M.P.; Legenstein, L.; Holzer, V.; Hofer, S.; Kaltenegger, M.; Resel, R.; Simbrunner, J. GIDInd: An Automated Indexing Software for Grazing-Incidence X-ray Diffraction Data. *J. Appl. Crystallogr.* **2021**, *54*, 1256–1267. https://doi.org/10.1107/S1600576721006609.
40. Bedlovičová, Z.; Strapáč, I.; Baláž, M.; Salayová, A. A Brief Overview on Antioxidant Activity Determination of Silver Nanoparticles. *Molecules* **2020**, *25*, 3191. https://doi.org/10.3390/molecules25143191.
41. Pyrzynska, K.; Pękal, A. Application of Free Radical Diphenylpicrylhydrazyl (DPPH) to Estimate the Antioxidant Capacity of Food Samples. *Anal. Methods* **2013**, *5*, 4288–4295. https://doi.org/10.1039/C3AY40367J.
42. Nilsson, J.; Pillai, D.; Önning, G.; Persson, C.; Nilsson, A.; Åkesson, B. Comparison of the 2,2′-Azinobis-3-Ethylbenzotiazo-Line-6-Sulfonic Acid (ABTS) and Ferric Reducing Anti-Oxidant Power (FRAP) Methods to Asses the Total Antioxidant Capacity in Extracts of Fruit and Vegetables. *Molecular Nutrition & Food Research* **2005**, *49*, 239–246.
43. Li, H.-B.; Wong, C.-C.; Cheng, K.-W.; Chen, F. Antioxidant Properties in Vitro and Total Phenolic Contents in Methanol Extracts from Medicinal Plants. *LWT Food Sci. Technol.* **2008**, *41*, 385–390. https://doi.org/10.1016/j.lwt.2007.03.011.
44. Panche, A.N.; Diwan, A.D.; Chandra, S.R. Flavonoids: An Overview. *J. Nutr. Sci.* **2016**, *5*, e47. https://doi.org/10.1017/jns.2016.41.
45. Gottshall, R.Y.; Lucas, E.H.; Lickfeldt, A.; Roberts, J.M. The Occurrence of Antibacterial Substances Active Against Mycobacterium Tuberculosis In Seed Plants. *J Clin Invest.* **1949**, *28*, 920–923. https://doi.org/10.1172/JCI102179.
46. Kryuchkov, M.; Adamcik, J.; Katanaev, V.L. Bactericidal and Antiviral Bionic Metalized Nanocoatings. *Nanomaterials* **2022**, *12*, 1868. https://doi.org/10.3390/nano12111868.
47. Ruby; Aryan; Mehata, M.S. Surface Plasmon Resonance Allied Applications of Silver Nanoflowers Synthesized from Breynia Vitis-Idaea Leaf Extract. *Dalton Trans.* **2022**, *51*, 2726–2736. https://doi.org/10.1039/D1DT03592D.
48. Padalia, H.; Moteriya, P.; Chanda, S. Green Synthesis of Silver Nanoparticles from Marigold Flower and Its Synergistic Antimicrobial Potential. *Arab. J. Chem.* **2015**, *8*, 732–741. https://doi.org/10.1016/j.arabjc.2014.11.015.
49. Mani, M.; Pavithra, S.; Mohanraj, K.; Kumaresan, S.; Alotaibi, S.S.; Eraqi, M.M.; Gandhi, A.D.; Babujanarthanam, R.; Maaza, M.; Kaviyarasu, K. Studies on the Spectrometric Analysis of Metallic Silver Nanoparticles (Ag NPs) Using Basella Alba Leaf for the Antibacterial Activities. *Environ. Res.* **2021**, *199*, 111274. https://doi.org/10.1016/j.envres.2021.111274.
50. Taleb Safa, M.A.; Koohestani, H. Green Synthesis of Silver Nanoparticles with Green Tea Extract from Silver Recycling of Radiographic Films. *Results Eng.* **2024**, *21*, 101808. https://doi.org/10.1016/j.rineng.2024.101808.
51. Li, S.; Shen, Y.; Xie, A.; Yu, X.; Qiu, L.; Zhang, L.; Zhang, Q. Green Synthesis of Silver Nanoparticles Using *Capsicum annuum* L. Extract. *Green Chem.* **2007**, *9*, 852–858. https://doi.org/10.1039/B615357G.
52. Aslam, M.; Fozia, F.; Gul, A.; Ahmad, I.; Ullah, R.; Bari, A.; Mothana, R.A.; Hussain, H. Phyto-Extract-Mediated Synthesis of Silver Nanoparticles Using Aqueous Extract of Sanvitalia Procumbens, and Characterization, Optimization and Photocatalytic Degradation of Azo Dyes Orange G and Direct Blue-15. *Mol. Basel Switz.* **2021**, *26*, 6144. https://doi.org/10.3390/molecules26206144.
53. Labulo, A.H.; David, O.A.; Terna, A.D. Green Synthesis and Characterization of Silver Nanoparticles Using *Morinda lucida* Leaf Extract and Evaluation of Its Antioxidant and Antimicrobial Activity. *Chem. Pap.* **2022**, *76*, 7313–7325. https://doi.org/10.1007/s11696-022-02392-w.
54. Jeeva, K.; Thiyagarajan, M.; Elangovan, V.; Geetha, N.; Venkatachalam, P. *Caesalpinia coriaria* Leaf Extracts Mediated Biosynthesis of Metallic Silver Nanoparticles and Their Antibacterial Activity against Clinically Isolated Pathogens. *Ind. Crops Prod.* **2014**, *52*, 714–720. https://doi.org/10.1016/j.indcrop.2013.11.037.
55. Shukla, V.K.; Yadav, R.S.; Yadav, P.; Pandey, A.C. Green Synthesis of Nanosilver as a Sensor for Detection of Hydrogen Peroxide in Water. *J. Hazard. Mater.* **2012**, *213–214*, 161–166. https://doi.org/10.1016/j.jhazmat.2012.01.071.
56. Nindawat, S.; and Agrawal, V. Fabrication of Silver Nanoparticles Using *Arnebia hispidissima* (Lehm.) A. DC. Root Extract and Unravelling Their Potential Biomedical Applications. *Artif. Cells Nanomed. Biotechnol.* **2019**, *47*, 166–180. https://doi.org/10.1080/21691401.2018.1548469.
57. Paterlini, P.; Rodríguez, C.; Ledesma, A.; Pereyra, J.; Dávila Costa, J.S.; Álvarez, A.; Romero, C.M. Characterization of Biosynthesized Silver Nanoparticles from *Streptomyces* Aqueous Extract and Evaluation of Surface-Capping Proteins Involved in the Process. *Nano-Struct. Nano-Objects* **2021**, *26*, 100755. https://doi.org/10.1016/j.nanoso.2021.100755.

58. Majeed Khan, M.A.; Kumar, S.; Ahamed, M.; Alrokayan, S.A.; AlSalhi, M.S. Structural and Thermal Studies of Silver Nanoparticles and Electrical Transport Study of Their Thin Films. *Nanoscale Res. Lett.* **2011**, *6*, 434. https://doi.org/10.1186/1556-276X-6-434.
59. Bruna, T.; Maldonado-Bravo, F.; Jara, P.; Caro, N. Silver Nanoparticles and Their Antibacterial Applications. *Int. J. Mol. Sci.* **2021**, *22*, 7202. https://doi.org/10.3390/ijms22137202.
60. Terzioğlu, E.; Arslan, M.; Balaban, B.G.; Çakar, Z.P. Microbial Silver Resistance Mechanisms: Recent Developments. *World J. Microbiol. Biotechnol.* **2022**, *38*, 158. https://doi.org/10.1007/s11274-022-03341-1.